

# Robust Microcapsules with Controlled Permeability from Silk Fibroin Reinforced with Graphene Oxide

Chunhong Ye, Zachary A. Combs, Rossella Calabrese, Hongqi Dai, David L. Kaplan, and Vladimir V. Tsukruk\*

**R**obust and stable microcapsules are assembled from poly-amino acid-modified silk fibroin reinforced with graphene oxide flakes using layer-by-layer (LbL) assembly, based on biocompatible natural protein and carbon nanosheets. The composite microcapsules are extremely stable in acidic (pH 2.0) and basic (pH 11.5) conditions, accompanied with pH-triggered permeability, which facilitates the controllable encapsulation and release of macromolecules. Furthermore, the graphene oxide incorporated into ultrathin LbL shells induces greatly reinforced mechanical properties, with an elastic modulus which is two orders of magnitude higher than the typical values of original silk LbL shells and shows a significant, three-fold reduction in pore size. Such strong nanocomposite microcapsules can provide solid protection of encapsulated cargo under harsh conditions, indicating a promising candidate with controllable loading/unloading for drug delivery, reinforcement, and bioengineering applications.

## 1. Introduction

Graphene, a one-atom thick layer of sp<sup>2</sup>-hybridized carbon atoms, has attracted attention in the broader scientific community because of its extraordinarily high electrical and thermal conductivities, excellent mechanical properties and high surface area.<sup>[1–4]</sup> Graphene has been explored for various applications in nanoelectronic and energy storage devices, ultra-sensitive materials, biomedical devices and as a critical component of nanocomposite materials.<sup>[5–9]</sup> However, graphene nanosheets are difficult to exfoliate and to process in aqueous and common organic solvents due to the strong

$\pi$ - $\pi$  interactions and van der Waals forces, which decrease the performance of devices and hinders the further development of graphene based structures.<sup>[10]</sup>

In contrast, graphene components can be easily dissolved in a variety of solvents after its conversion to graphene oxide (GO) which further helps in improving interfacial interactions.<sup>[11,12]</sup> Graphene oxide nanosheets can be synthesized from graphite flakes by thermal oxidation in a controlled, scalable and reproducible manner with a high density of epoxide and hydroxyl groups at in-plane binding sites and carboxyl groups around the edges, enabling stable aqueous processibility and enhancement of interfacial interactions and cross-linking.<sup>[11,13]</sup> Graphene oxide exhibits potential as a solution-processable, flexible material, for fabricating graphene-based composites due to its outstanding mechanical properties, flexible 2D structure, high binding potential and single/double atomic layers that can easily turn into a conductive reduced-graphene oxide (rGO) form.<sup>[14–17]</sup> Bio-medical applications such as drug/gene delivery and biocomposites with high colloidal stability and biocompatibility have been reported.<sup>[18–20]</sup> Importantly, in spite of structural defects, the elastic modulus of graphene oxide is still very high, around 0.25 TPa.<sup>[21,22]</sup> Furthermore, graphene oxide nanosheets have been considered to be excellent two-dimensional fillers for polymer nanocomposites with outstanding mechanical strength, along with the potential for excellent electrical and thermal properties. For example, GO-polyelec-

Dr. C. Ye, Prof. H. Dai  
School of Light Industry Science and Engineering  
Nanjing Forestry University  
Nanjing, Jiangsu 210037, PR China  
Dr. C. Ye, Dr. Z. A. Combs, Prof. V. V. Tsukruk  
School of Materials Science and Engineering  
Georgia Institute of Technology  
Atlanta, Georgia 30332, USA  
E-mail: Vladimir@mse.gatech.edu  
Dr. R. Calabrese, Prof. D. L. Kaplan  
Department of Biomedical Engineering  
Tufts University  
4 Colby street, Medford, MA 02155, USA  
DOI: 10.1002/sml.201401119



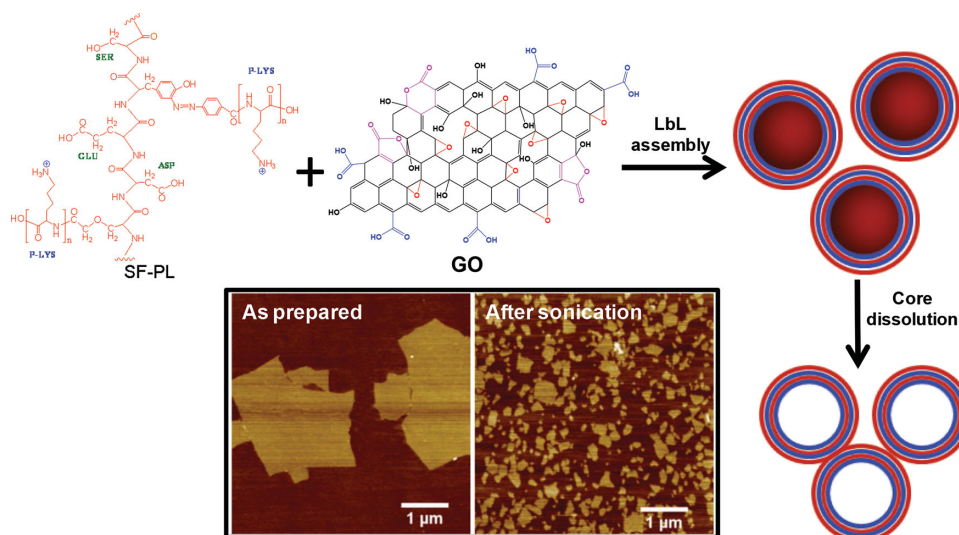


**Figure 1.** The fabrication of graphene oxide/silk ionomer LbL microcapsules. The AFM topographical image shows the lateral dimension and morphology of graphene oxide flakes as prepared and after additional sonication treatment, z-scale: 4 nm.

trolyte nanomembranes have demonstrated high toughness of  $1.9 \text{ MJ/m}^3$  and high elastic modulus of about 20 GPa.<sup>[23]</sup>

Our recent study demonstrated silk fibroin-graphene oxide nanocomposite membranes with remarkable mechanical properties, including a tensile modulus of 145 GPa, an ultimate stress of more than 300 MPa and a toughness of  $2.2 \text{ MJ/m}^3$ , many-fold higher than those previously reported.<sup>[24]</sup> However, to date, only a few examples utilizing graphene oxide for preparing 3D structures, such as microcapsules, have been reported. Severe aggregation and polydispersity in size of the graphene-based capsules hindered further development.<sup>[25–29]</sup> Furthermore, some critical properties, such as permeability and mechanical properties of corresponding composite microcapsules for potential applications in drug delivery and biosensors have not been addressed in detail.

Herein, we report the fabrication of individual monodisperse composite microcapsules based on graphene oxide nanosheets and silk fibroin ionomer modified with poly-(L-lysine) by employing a facile layer-by-layer (LbL) assembly.<sup>[30–34]</sup> The microcapsules exhibited pH-controllable permeability and showed extreme stability in acidic (pH 2.0) and basic (pH 11.5) conditions without noticeable disintegration. Accompanying the tunable permeability, the silk fibroin and graphene oxide nanocomposite shells exhibited remarkable mechanical properties, with an elastic modulus of 470 MPa, which is two orders of magnitude higher than that measured for pure silk-based microcapsules. Moreover, the porosity of composite microcapsules has been significantly reduced due to the presence of the overlapped graphene oxide flakes in comparison with extremely permeable silk-based microcapsules.

## 2. Results and Discussion

### 2.1. Fabrication of $(\text{SF-PL/GO})_n$ Microcapsules

Composite microcapsules fabricated from graphene oxide nanosheets and functionalized natural protein,

silk-poly-(L-lysine), utilize two components to facilitate ionic pairing to reinforce ultrathin LbL shells (**Figure 1**). The water-soluble graphene oxide sheets prepared by the oxidative exfoliation of graphite flakes show homogeneous dispersions and are enriched with epoxide, hydroxyl, carbonyl and carboxyl groups on the surface for aqueous assembly, interfacial interactions and cross-linking.<sup>[46]</sup> The flakes had a micro-scale lateral size that could be controlled by sonication. AFM images revealed planar flakes with a size of several micrometers broken into smaller pieces ( $<500 \text{ nm}$ ) after sonication (**Figure 1**). The sheets had a thickness of  $1.0 \pm 0.1 \text{ nm}$ , in agreement with previously reports and indicate the presence of predominantly single/double flakes.<sup>[23,47]</sup>

In order to monitor the stepwise growth of the SF-PL/GO multilayer assembly on silica spheres, the  $\zeta$ -potential for the particles after each deposition step was measured (**Figure 2**). At the LbL assembly condition (pH  $\sim 5.5$ ), graphene oxide is negatively charged according to the  $\text{pK}_a$  of the carboxyl

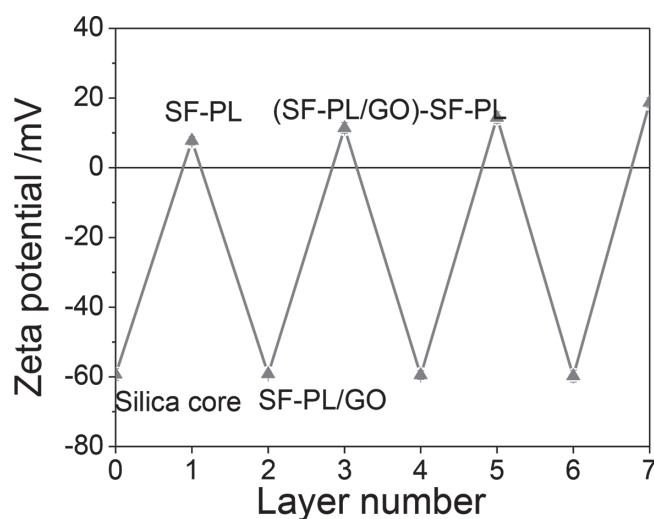


**Figure 2.** Stepwise zeta-potential variation during the LbL assembly of  $(\text{SP-PL/GO})_n$  shell on silica spheres.

groups,  $\sim 3.75$ ,<sup>[48]</sup> whereas the SF-PL is positively charged ( $pK_a$  of poly-lysine is  $\sim 9$ ).<sup>[49]</sup> The original silica spheres have a  $\zeta$ -potential of about  $-59$  mV. After the first layer deposition of SF-PL, the  $\zeta$ -potential dramatically increased to positive values ( $\sim 8$  mV). Following the assembly of the GO layer, the  $\zeta$ -potential correspondingly changed to the negative value again. The alternating positive/negative  $\zeta$ -potential of the silica particles after each SF-PL and GO deposition indicated a common charge-overcompensated mechanism of LbL shell formation based on electrostatic forces, suggesting the successful stepwise growth of hybrid SF-PL/GO shells onto the silica spheres.<sup>[49]</sup>

## 2.2. Morphology (SF-PL/GO)<sub>n</sub> Microcapsules

Next, we investigated the morphology of the decorated silica particles and hollow shells after dissolution of the silica core (Figure 3). Confocal microscopy images of the microcapsules stained with FITC showed uniform spherical shapes with a diameter around  $3.7 \mu\text{m}$ , close to the original core dimension and duplicating the core shape (Figure 3b), suggesting the thin shells of (SF-PL/GO)<sub>n</sub> were robust enough to preserve the spherical geometry after core dissolution. The SEM images revealed roughened surfaces of silica spheres after the assembly of the graphene oxide/silk ionomer shells. After core dissolution, the hollow dry capsules collapsed and showed random wrinkles caused by drying, which is common for uniform compliant shells (Figure 3c,e).<sup>[50,51]</sup> In contrast to previously reported silk based capsules with grainy topography,<sup>[43]</sup> high-resolution AFM images of the hybrid (SF-PL/GO)<sub>n</sub> capsules demonstrated a textured morphology with many large-scale wrinkles associated with the randomly folded flexible GO nanosheets (Figure 3d,f). The TEM images of shells confirmed the hollow structure of the capsules after the silica core was dissolved (Figure 4a). High resolution TEM images revealed uniform morphology of the hollow shells with many large and small wrinkles, which is a characteristic morphology of graphene oxide nanocomposites (Figure 4b).<sup>[25]</sup>

Next, Raman spectra were collected directly from the microcapsules to confirm the presence of the graphene oxide in the shells (Figure 4c, d). The spectra of the microcapsules showed typical graphene oxide active bands with a characteristic peak around  $1362 \text{ cm}^{-1}$  attributed to the D-band

and the peak at  $1599 \text{ cm}^{-1}$  that corresponds to the G-band (Figure 4c).<sup>[52]</sup> Meanwhile, Raman mapping of composite microcapsules obtained by integrating the intensity of the peak from the G-band demonstrated the uniform distribution of GO nanosheets over the entire surface of the microcapsules, with concentrated materials within wrinkles with folded sheets (Figure 4d). The  $I_D/I_G$  ratio was 1.77 which is consistent with that previously reported for graphene oxide sheets with high concentrations of defects and oxygenated regions.<sup>[13,53]</sup>

The thickness of (SF-PL/GO)<sub>n</sub> composite microcapsules with a different number of bilayers were measured from

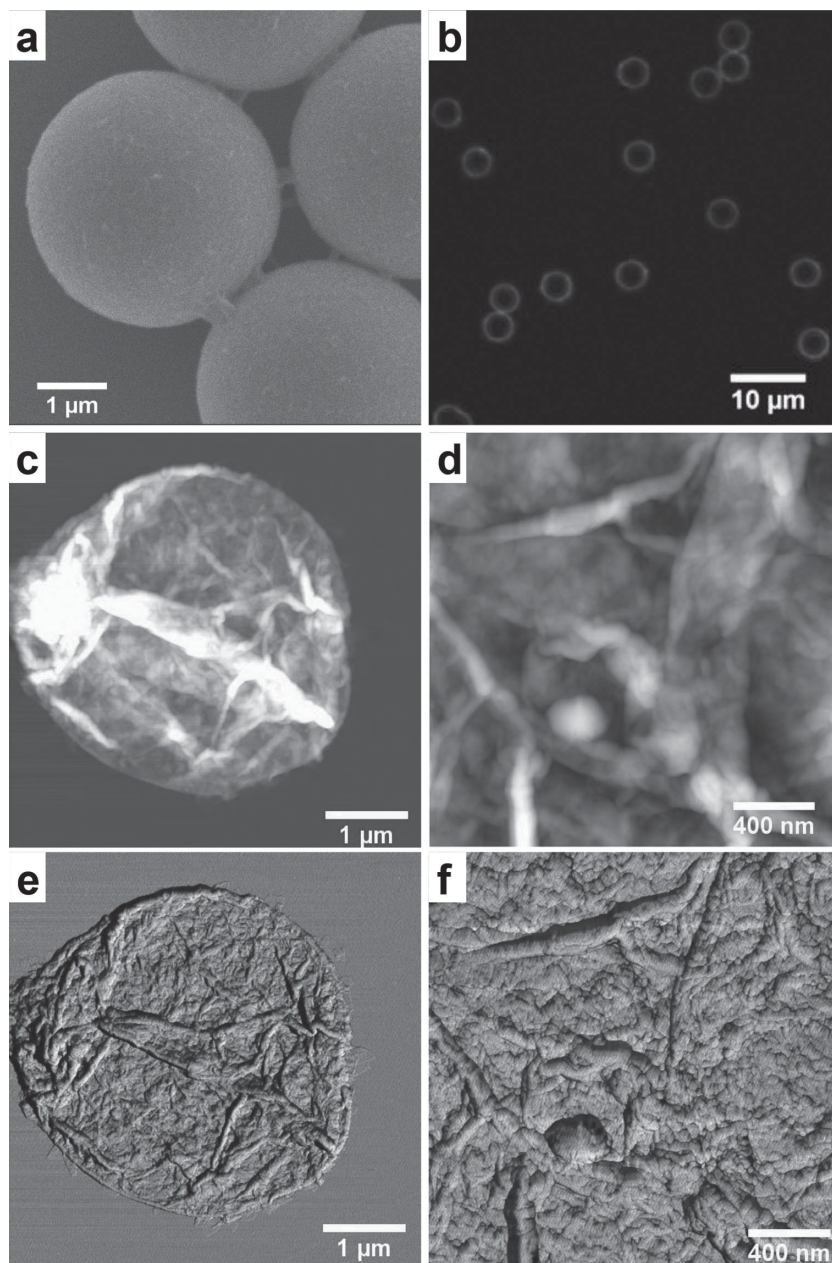


**Figure 3.** Morphology of microcapsules LbL assembled with graphene oxide and silk ionomer components. (a) SEM image of (SP-PL/GO)<sub>3.5</sub> capsule with silica core; (b) Confocal image of (SP-PL/GO)<sub>3.5</sub> capsule shell labeled with FITC; (c) AFM topography image (c) and corresponding phase image (e) of hollow (SP-PL/GO)<sub>3.5</sub> capsule in dry state (Z-scale: 300 nm and 40°); (d, f) High resolution AFM height and phase images of capsule shell (Z-scale: 250 nm and 40°).

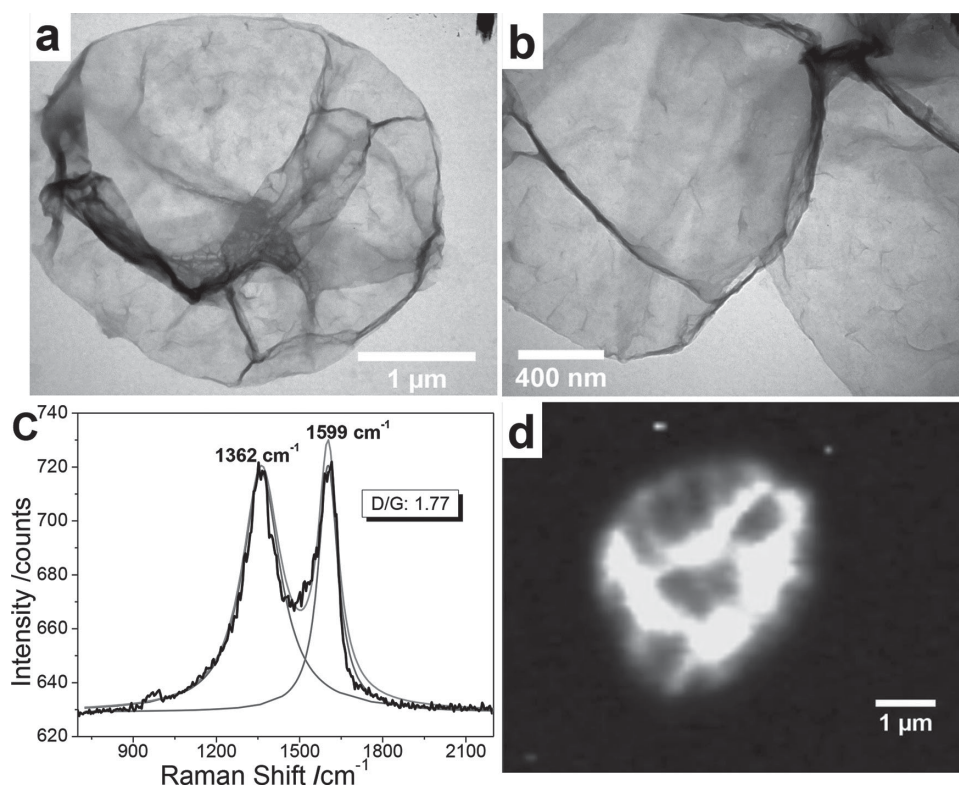


**Figure 4.** (a) The TEM image of GO-silk ionomer microcapsule; (b) High resolution TEM images taken at the edge of a microcapsule; (c) Raman spectra collected from the microcapsule; (d) Raman mapping of the graphene oxide G-band ( $1599\text{ cm}^{-1}$ ) for individual microcapsule.

AFM cross-sections in the dry state after removal of the silica cores (**Figure 5**). The shell thickness increased from  $5 \pm 0.5\text{ nm}$  to  $23 \pm 2\text{ nm}$  with an increasing number of bilayers, another confirmation of the organized LbL assembly (**Figure 5i**). The average increment for each SF-PL/GO bilayer was around  $5.7\text{ nm}$ , which was slightly higher than the known value of silk-on-silk shells based on hydrophobic interactions and planar LbL films ( $3.5\text{ to }5\text{ nm}$ ).<sup>[54–56]</sup> Unlike the microcapsules fabricated by homogeneous silk ionomers with exponential growth, the hybrid (SF-PL/GO)<sub>n</sub> shells exhibited linear growth, suggesting the silk ionomer/GO only adsorbed on the top of the outmost layers with limited interlayer diffusion,<sup>[57,58]</sup> which can be ascribed to impermeable graphene oxide nanosheets. Correspondingly, the collapsed hollow capsules showed fewer large-scale wrinkles with increasing bilayer numbers due to increasing shell stiffness (**Figure 5a–d**).

High-resolution AFM of hollow shells demonstrated significant changes in the shell topography from a relatively smooth surface to rough and aggregated morphologies with increasing bilayer numbers (**Figure 5e–h**). The wall microroughness increased from  $3.8$  to  $8.4\text{ nm}$  with an increasing number of bilayers as measured in a selected area of  $1 \times 1\ \mu\text{m}^2$  (**Figure 5i**). These higher values are caused by the presence of random fine wrinkles and agree with previously reported silk/GO materials and other composite LbL films.<sup>[24]</sup> Microroughness is much higher than common values for traditional electrostatic polymeric LbL films, which are usually well below  $1\text{ nm}$ .<sup>[24]</sup>

### 2.3. LbL Shell Permeability

The highly aggregated surface of the microcapsules suggested a potentially porous morphology of the LbL shells. Thus, we examined the permeability of the composite (SF-PL/GO)<sub>3.5</sub> microcapsules at different pH conditions by employing green fluorescent FITC-dextran with various molecular weights as probes (**Figure 6**).<sup>[59,60]</sup> Instead of investigating the effect of shell thickness on permeability which is well known for LbL shells,<sup>[43,54,61]</sup> we focused on studying shell permeability as a function of the surrounding pH since the silk ionomer component is pH-sensitive. We observed that the composite microcapsules with 3.5 bilayer shells were permeable to almost all of the dextrans at pH 2.0, except to a molecular weight of  $2000\text{ kDa}$  (**Figure 6a–c**). Increasing pH resulted in a decrease in cutoff molecular weight to  $500\text{ kDa}$  for neutral conditions and a further reduction of the cutoff threshold to  $250\text{ kDa}$  at very basic conditions (**Table 1**). The phenomenon is in a striking contrast with previously reported homogeneous silk ionomer microcapsules, where the permeability was significantly increased in acidic and basic conditions and pore sizes were much larger thus facilitating permeability of large macromolecules regardless of environmental conditions.<sup>[43]</sup>

The reported hydrodynamic diameters of the FITC-dextran macromolecules with different molecular weights of  $250$ ,  $500$  and  $2000\text{ kDa}$  are  $11.5$ ,  $15.9$  and  $26.9\text{ nm}$ , respectively.<sup>[62]</sup> Therefore, we estimated the mesh size of porous (SF-PL/GO)<sub>3.5</sub> shells at pH 2.0 to be around  $27\text{ nm}$ ,

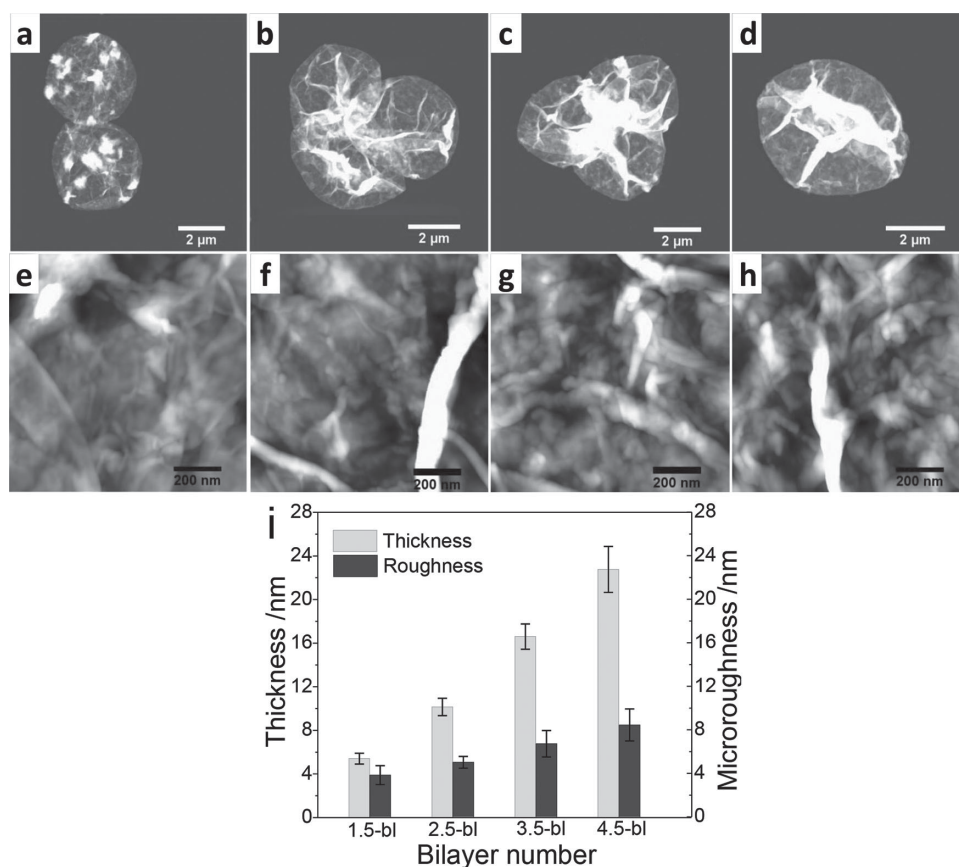


**Figure 5.** AFM topographical images of (SF-PL/GO)<sub>n</sub> microcapsules (top row) and high resolution shell topography (bottom row) of (SF-PL/GO)<sub>n</sub> microcapsules with different bilayer number, 1.5 bilayer (a, e), 2.5 bilayer (b, f), 3.5 bilayer (c, g) and 4.5 bilayer (d, h), Z-scale: 200 nm (a), 30 nm (b), 400 nm (c, d) and 80 nm (e, f, g, h); (i) Variation of shell thickness and microroughness of (SF-PL/GO)<sub>n</sub> microcapsules as a function of bilayer numbers.

which is close to but lower than that of the (SF-PL/GO)<sub>3.5</sub> shells with 32 nm pore size in neutral pH (larger pores showed up as exposed to acidic and basic conditions).<sup>[43]</sup> Moreover, the pore size of the GO-silk shells was further reduced by more than a factor 2 to 11.5 nm at increasing pH (Table 1). In short, the porosity of the GO-silk shells can be controlled by pH conditions and significantly reduced in contrast to pure silk shells.

The pH-dependent changes of permeability for composite (SF-PL/GO)<sub>3.5</sub> microcapsules can be attributed to the transformation of the secondary structure of silk-poly-(L-lysine) at various pHs.<sup>[63]</sup> In acidic conditions, the higher charge density of the SF-PL contributes to extended molecular chains.<sup>[64]</sup> As pH is increased, the positive charges of the SF-PL are gradually reduced due to deprotonation of the amino groups with an isoelectric point in basic conditions ( $pK_a$  is 9).<sup>[49]</sup> Correspondingly, the SF-PL backbones are transformed to random coils as associated with the decrease of charge density.<sup>[64]</sup> Therefore, the shrinkage of SF-PL molecule chains contributed to the gradual densification of the shells and the reduction in shell porosity with increasing pH values.

Furthermore, it is worth noting that the (SF-PL/GO)<sub>3.5</sub> microcapsules did not show any significant swelling behavior at extremely acidic (pH 2.0) and basic (pH 11.5) conditions in comparison to the dramatic volume swelling (up to 800%) of homogeneous silk ionomer capsules in our previous report

(Figure 6).<sup>[43]</sup> This difference can be ascribed to the presence of strong, overlapped, and folded graphene oxide nanosheets that limit the swellability of the silk matrix and serve as efficient physical crosslinkers. Indeed, unlike the capsules composed of silk ionomer-on-silk ionomer with intense interfacial diffusion of polymer networks,<sup>[58,65]</sup> the reinforced SF-PL/GO shells are composed of tightly stacked, folded, and wrapped nanosheets with silk chains. Moreover, aside from ionic pairing between GO and SF-PL chains, hydrogen bonding among nanosheets with oxygenated patches and multidomain silk fibroin, contribute to the stability of composite (SF-PL/GO)<sub>3.5</sub> shells in harsh pH conditions.<sup>[66]</sup>

#### 2.4. Mechanical Stability of the Hollow Microcapsules

Finally, we conducted osmotic pressure measurements to assess the mechanical stability of the composite microcapsules under external pressure. For these studies, 2,000 kDa FITC-labeled dextran solutions with different concentrations were chosen to induce an external osmotic pressure because of the stability to osmotic pressure regardless of the pH, temperature or ions and impermeability of the shells to this molecular weight.<sup>[67,68]</sup> Microcapsule shells work as a semi-permeable membrane, which is permeable for the solvent (H<sub>2</sub>O), but impermeable to the large molecular weight

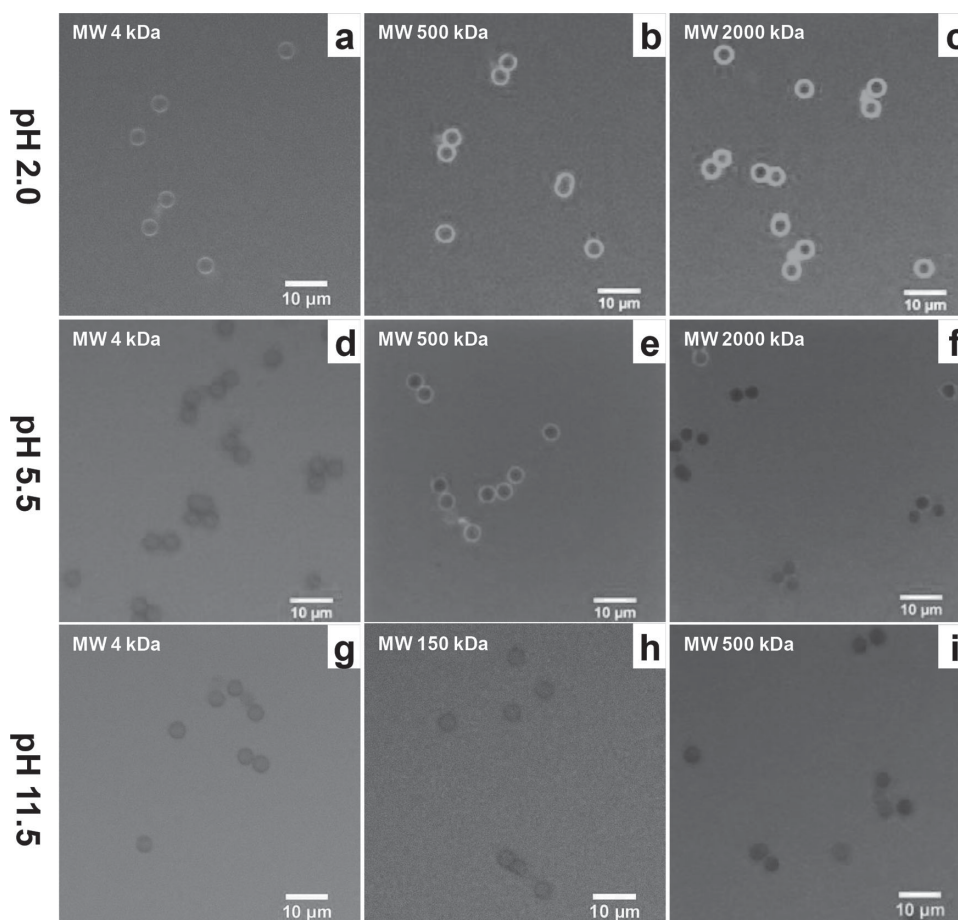


**Figure 6.** Permeability of (SP-PL/GO)<sub>3,5</sub> microcapsules to FITC-labeled dextrans with various molecular weight at different pHs. Confocal images of (SP-PL/GO)<sub>3,5</sub> exposed to FITC-Dextran solution with different molecular weights at pH 2.0 (a, b, c); pH 5.5 (d, e, f) and pH 11.5 (g, h, i).

macromolecules in the external bulk solution. The difference in dextran concentration between the exterior and interior of microcapsules resulted in osmotic pressure, which can be easily estimated.<sup>[69]</sup> When the osmotic pressure is above a critical pressure ( $P_{cr}$ ), the shells cannot sustain the rising hydrostatic pressure and buckle.<sup>[70]</sup> Indeed, progressing buckling was observed for both 4 and 5 bilayer PEI-(SF-PG/SF-PL) shells and (SF-PL/GO)<sub>4,5</sub> shells at increasing dextran solution concentrations (**Figure 7**, **Figure 8**). The microcapsules prepared from silk ionomers without graphene oxide flakes kept uniform spherical shapes in 2% dextran solution (Figure 7a,d). Increasing the concentration of dextran up to 4% resulted in partial deformation of the capsules, and at 12% dextran concentration almost 100% of the capsules finally collapsed (Figure 7b-f).

**Table 1.** Permeability of (SP-PL/GO)<sub>3,5</sub> microcapsules to FITC-dextran compounds with different molecular weights in phosphate solution at pH 2.0, 5.5 and 11.5.

MW pH	4 kDa	10 kDa	20 kDa	150 kDa	250 kDa	500 kDa	2000 kDa
2.0	+	+	+	+	+	+	±
5.5	+	+	+	+	+	±	-
11.5	+	+	+	+	±	-	-

Symbols "+", "-" and "±" indicate permeable, impermeable and partially permeable capsules, respectively.

In contrast, the composite microcapsules fabricated with silk ionomers and graphene oxide showed remarkable stability even at very high concentrations of dextran solution (Figure 8). The microcapsules retained their uniform spherical shape without noticeable buckling over a wide range of dextran concentrations from 0 to 25% (Figure 8 a,b,d). Even when the dextran concentration reached 30%, only partial buckling occurred (Figure 8c, e), suggesting much higher mechanical stability of the reinforced microcapsules. The deformation of the capsules in dextran solution with higher concentrations could not be monitored because of the high viscosity of the concentrated solution.

For quantitative analysis of shell deformation, the percentage of collapsed capsules was plotted versus the concentration of dextran solution (Figures 7, 8). A common sigmoidal curve was obtained for the control pure silk PEI-(SF-PG/SF-PL)<sub>n</sub> capsules (Figure 7g). At lower dextran concentrations, the osmotic pressure did not deform the microcapsules. As the concentration of dextran increased, the microcapsules started to deform due to the increased osmotic pressure and then buckled in a concentration region from 2% to 6% for silk ionomer based capsules with 4 and 5 bilayers with modest variability.<sup>[70]</sup> To obtain mean critical osmotic pressure for specific microcapsules, the dextran concentration which caused 50% capsule deformation was defined as the transition point, and the corresponding osmotic pressure was defined as the critical

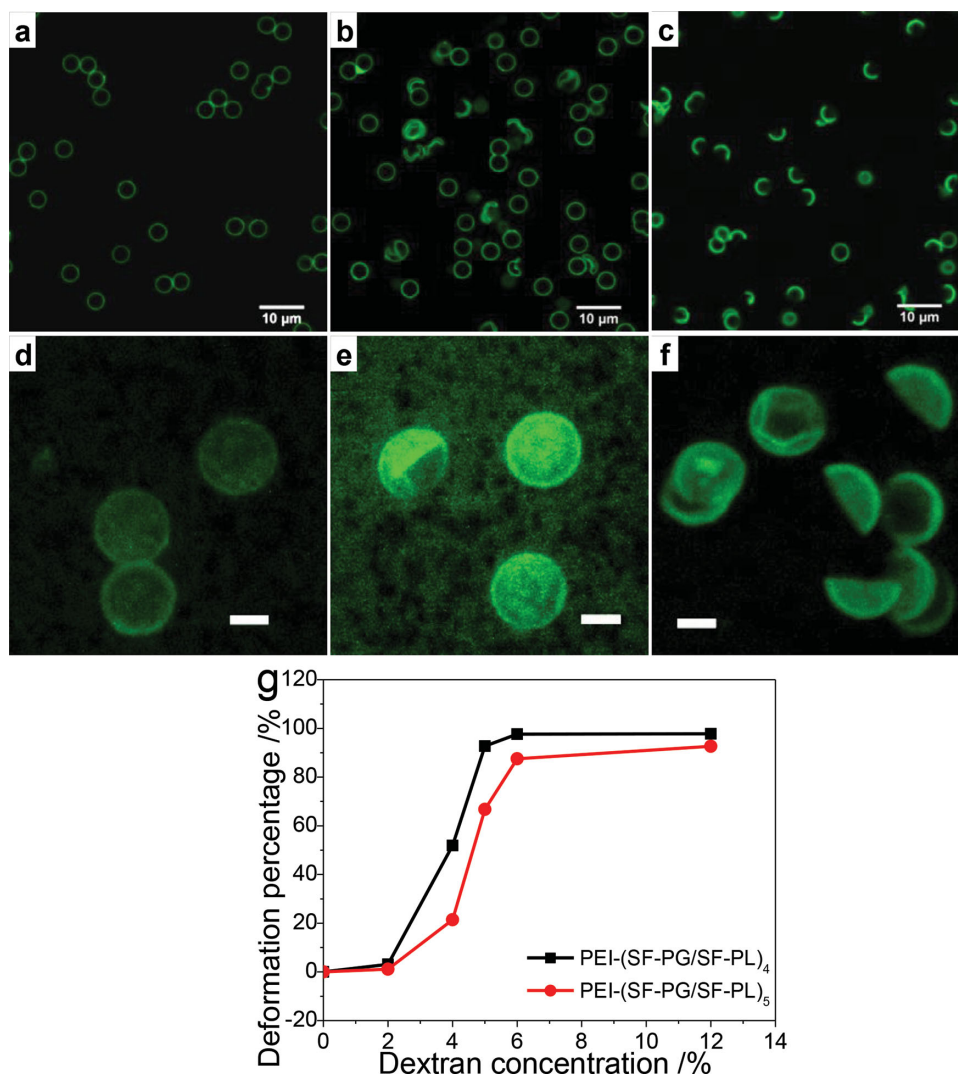


**Figure 7.** Cross section (top row) and reconstructed 3D (bottom row) confocal images of PEI-(SF-PG/SF-PL)<sub>5</sub> cross-linked microcapsules exposed to 2000 kDa Dextran with different concentrations, 2% (a, d), 4% (b, e) and 12% (c, f), at pH 5.5, scale bar: 10  $\mu\text{m}$  (a, b, c), and 2  $\mu\text{m}$  (d, e, f); (g) Percentage of collapsed microcapsules as a function of dextran concentration.

pressure.<sup>[71]</sup> Thus, the transition points were estimated from the deformation-concentration curves as 3.9% and 4.6% for 4- and 5-bilayer PEI-(SF-PG/SF-PL) capsules, respectively.<sup>[70]</sup>

However, sigmoidal deformation-concentration curves were not obtained for the reinforced microcapsules (SF-PL/GO)<sub>4,5</sub> up to the highest achievable concentration of 30% (Figure 8f). The graphene oxide based composite microcapsules indicated good stability even in 25% dextran solution and at a 30% dextran concentration, 32% of all capsules are deformed. To evaluate the critical osmotic pressure, the extrapolation to higher dextran concentrations was conducted based on the deformation data (Figure 8f). According to the dextran concentration obtained at the transition point from the deformation-concentration curve, corresponding osmotic pressure can be calculated by using a polynomial expression suggested from analysis of experimental results:<sup>[68,72,73]</sup>

$$P = 286c + 87c^2 + 5c^3 \quad (1)$$

where  $c$  is dextran concentration in weight percentage. The transition point for reinforced (SF-PL/GO)<sub>4,5</sub> microcapsules was estimated from this analysis to be 33%, which is several-folds higher than the value of pure silk ionomers based microcapsules. Furthermore, the effect of cross-linking was investigated by comparing the deformation of (SF-PL/GO)<sub>3,5</sub> capsules with and without cross-linking at different dextran concentrations (Figure 8f). The deformation limit of capsules without cross-linking is slightly higher than that of cross-linked capsules, consistent with previously reported studies in which cross-linking contributed to the enhanced mechanical properties.<sup>[61,74]</sup> However, this deformation percentage of non cross-linked silk-graphene oxide composite shells is low compared to the cross-linked pure silk ionomers based capsules, indicating that graphene oxide sheets work as a major reinforcing factor of the strong mechanical properties of (SF-PL/GO)<sub>n</sub> shells.

The theory of mechanical stability of elastic thin layers under external stresses allows for the estimation of the limits

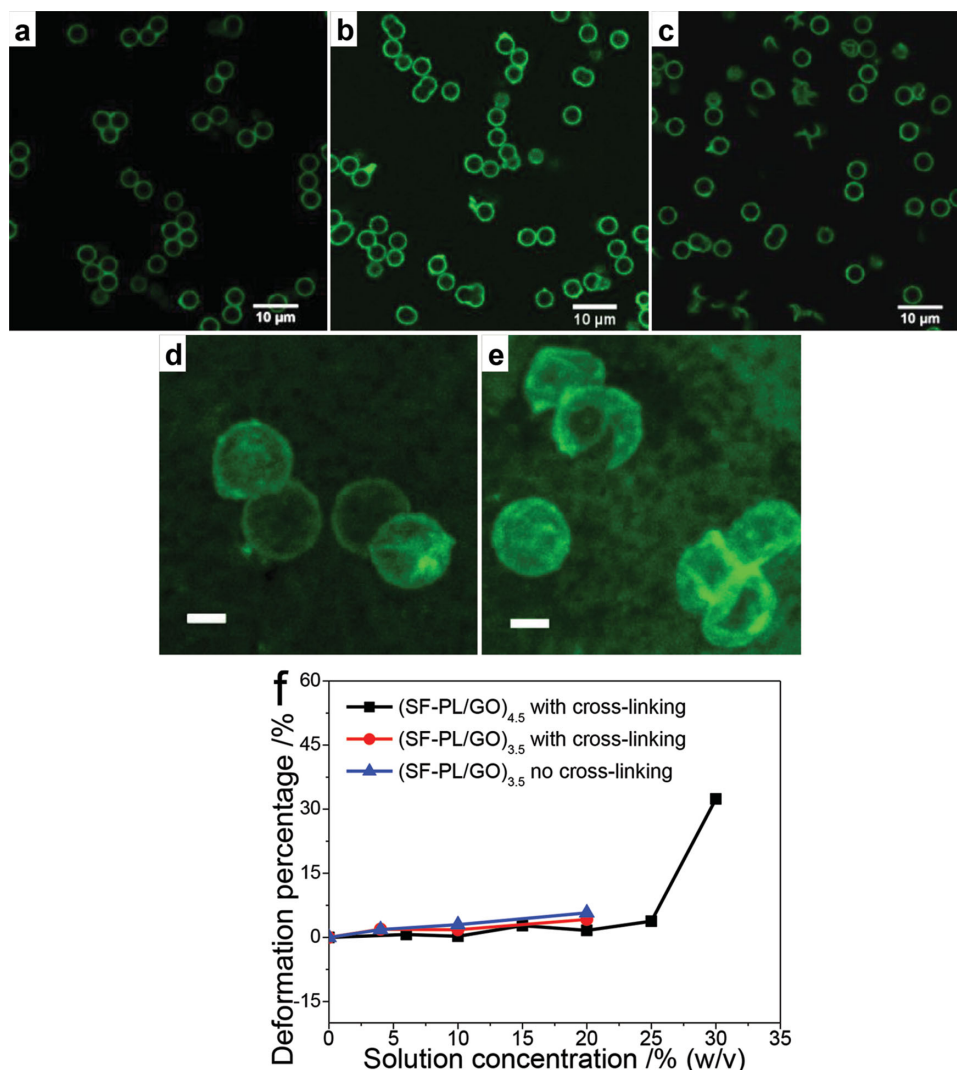


**Figure 8.** Cross section (top row) and reconstructed 3D (bottom row) confocal images of (SF-PL/GO)<sub>4,5</sub> hybrid microcapsules exposed to 2000 kDa Dextran with different concentrations, 10% (a), 15% (d), 20% (b) and 30% (c, e), at pH 5.5, scale bar: 10 μm (a, b, c) and 2 μm (d, e); (f) Percentage of collapsed (SF-PL/GO)<sub>3,5</sub> microcapsules with/without cross-linking as a function of the dextran concentration.

of shell stability under the osmotic pressure by finding a critical stress,  $P_{cr}$ , from the known expression:<sup>[75,76]</sup>

$$P_{cr} = \frac{2E}{\sqrt{3(1-\nu^2)}} \left( \frac{\delta}{R} \right)^2 \quad (2)$$

where  $E$  is composite Young's modulus of the shell, which is related to tensile elastic modulus,  $\nu$  is the Poisson's ratio and 0.5 for incompressible elastic material,  $\delta$  is the thickness of the shell and  $R$  is the radius of the microcapsules. The critical pressure required for inducing microcapsule buckling is proportional to the shell thickness and is inversely proportional to the capsule radius. This equation was verified for calculating the elastic modulus of microcapsules by varying capsule thickness and radius as reported in literature.<sup>[70,71]</sup>

Based upon this theory, the calculated critical osmotic pressures were 2.7 kPa, 3.6 kPa and 286 kPa, for PEI-(SF-PL/SF-PG)<sub>4</sub>, PEI-(SF-PL/SF-PG)<sub>5</sub> and (SF-PL/GO)<sub>4,5</sub>, respectively. Furthermore, the calculated elastic modulus

value in the swollen state was within 1.5 – 1.6 MPa for purely silk microcapsules with 4 and 5 bilayers. These values are comparable but lower than that previously reported for silk ionomer capsules (around 8.5 MPa) from surface force spectroscopy<sup>[61]</sup> This difference can be related to the fact that AFM measures localized compressive modulus in contrast to microscopic bending stability tested with osmotic measurements in this study. On the other hand, these values are close to the elastic modulus of approximately 1 MPa reported for polyelectrolyte multilayer films with natural components such as chitosan/hyaluronan, poly-L-lysine/hyaluronan and poly (allyamine hydrochloride)/poly-L-glutamic acid from AFM nanoindentation.<sup>[77]</sup> Overall, the stiffness of hollow LbL microcapsules depended on the degree of cross-linking time,<sup>[78]</sup> molecular weight,<sup>[79]</sup> template dissolution,<sup>[80]</sup> and pH.<sup>[61]</sup> For instance, the elastic modulus of hydrogen-bonded shells based on single poly (methacrylic acid)-co-NH<sub>2</sub> component or tannic acid/poly-vinylpyrrolidone (TA/PVPON) varied in the range of 0.7 to 5 MPa with different cross-linking time and templates. On the other hand, significantly higher

elastic moduli for ionic PSS/PDADMAC and hydrogen-bonded PMAA/PVPON shells were reported within the range of 100–600 MPa and related to modest swelling of these shells with high crosslinking density.<sup>[71,81–83]</sup>

Finally, the calculated elastic modulus for reinforced silk-graphene oxide shells was dramatically higher, around 470 MPa. This value is more than two orders of magnitude higher than the pure silk ionomer shells, indicating remarkable reinforcement of shell mechanical strength after incorporation of graphene oxide flakes, exceeding typical values for swollen purely polymeric or protein LbL shells.<sup>[84,85]</sup> However, considering the overall content of graphene oxide (about 20%) we can conclude the mechanical stability is still lower than that expected from the properties of individual components. We suggest that the random morphology of composite shells with wrinkled and folded graphene oxide flakes is responsible for the reduced reinforcement. Also, the reduced but still significant porosity of the GO-silk shells contributes to this effect as well. These properties are in contrast to highly ordered, dense, and tightly stacked silk-graphene oxide nanocomposites facilitated by spin-assisted LbL assembly with very high elastic modulus.<sup>[24]</sup>

### 3. Conclusions

Robust and mechanically stable composite microcapsules were successfully fabricated from silk ionomers and graphene oxide nanosheets. The capsules were stable even under extreme acidic (pH 2) and basic (pH 11.5) conditions, and demonstrated pH-tunable permeability, which can facilitate pH-controlled encapsulation and release of large macromolecules in contrast to pure silk microcapsules. These composite microcapsules possessed dramatically increased elastic moduli of about 0.5 GPa (as compared to about 2 MPa for pure silk microcapsules) and reduced permeability with pores size down to 11 nm (from about 32 nm pores in purely silk microcapsules), due to the presence of strong, flexible, and overlapped graphene oxide flakes. Such robust silk-graphene oxide hybrid nanocomposite microcapsules exhibit a promising platform for drug delivery, cell surface engineering and biosensors under demanding environmental conditions.<sup>[86]</sup>

### 4. Experimental Section

**Microcapsule Fabrication:** Graphene oxide (GO) suspension (concentration: 0.15%, w/w) was synthesized from natural graphite flakes (325 mesh, 99.8% metal basis) purchased from Alfa Aesar using the Hummer's method.<sup>[11,35]</sup> The condensed graphene oxide was redispersed in water (0.5 mg/mL). Poly(amino acid) modified silk ionomers, silk-poly-L-lysine (SF-PL) and silk-poly-L-glutamic acid (SF-PG), were synthesized according to our previously published method.<sup>[36]</sup> Briefly, *Bombyx mori* cocoons were degummed by boiling in 0.2 M Na<sub>2</sub>CO<sub>3</sub> to remove sericin.<sup>[37]</sup> The poly-L-lysine and poly-L-glutamic acid were grafted onto the silk fibroin backbone obtaining silk-poly-L-lysine (SF-PL) with high content of amine group and silk-poly-L-glutamic acid (SF-PG) with

high degree of carboxyl groups as characterized by NMR (see earlier publication)<sup>[36]</sup> (Figure 1).

As sacrificial cores, 4.0 ± 0.2 μm diameter silica microspheres as 10% dispersions in water were purchased from Polysciences. Sodium phosphate dibasic, sodium phosphate monobasic, and hydrofluoric acid (HF 48–51%) were obtained from VWR International. Ammonium fluoride (AF) was from Alfa Aesar. Fluorescent isothiocyanate (FITC) and different molecular weights dextrans labeled with FITC were obtained from Sigma-Aldrich. The zero-distance cross-linker, 1-ethyl-3-[3-dimethylaminopropyl] carbodiimide hydrochloride (EDC), was purchased from TCI.<sup>[38,39]</sup> Single-side polished silicon wafers (100 orientation, University Wafer Co) were cut to a typical size of 10 mm × 20 mm and cleaned with piranha solution according to previous publication.<sup>[40]</sup> All the materials were used as purchased. The water used in all experiments with a resistivity above 18.2 MΩ·cm from Barnstead Nanopure water system.

Silk-poly-L-lysine was deposited onto silica spheres in 1 mg/mL SF-PL solution, prepared in 0.05 M phosphate buffer with pH 5.5, for 15 min with gently rotation, followed by two wash cycles by phosphate buffer with pH 5.5 and centrifugation to remove the excess polyelectrolyte. The graphene oxide deposition was then carried out by redispersion in 0.5 mg/mL GO aqueous suspension, and washed by Nanopure water twice as the same procedure described above. Multilayered shells were deposited on the silicon templates by repeating the alternating deposition of SF-PL and GO components (Figure 1). In addition, covalent cross-linking was introduced between GO and SF-PL utilizing 1-ethyl-3-[3-dimethylaminopropyl] carbodiimide hydrochloride (EDC) as a cross-linking agent to avoid the disintegration of the capsules according to established procedures.<sup>[38]</sup> The silica spheres with alternating SF-PL/GO multilayers were added to EDC solution (5 mg/mL, prepared in 0.05 M phosphate buffer at pH 5.5), redispersed and rotated for 40 min, then excess coupling agent was washed out by phosphate buffer with pH 5.5. The silica cores were dissolved by exposing to HF/NH<sub>4</sub>F solution (pH ≈ 5.5) overnight, followed by dialysis against Nanopure water at pH 5.5 for 72 h (Figure 1).<sup>[41,42]</sup> All the procedures were carried out at mild pH (~5.5) to maximize to stabilize capsules.

The silk-poly(amino acid)-based ionomer microcapsules, PEI-(SF-PG/SF-PL)<sub>n</sub>, were prepared according to our previous publication<sup>[43]</sup> for comparing the mechanical properties with the hybrid (SF-PL/GO)<sub>n</sub> microcapsules. The chemically modified silk fibroin counterparts, silk-poly-L-lysine (SF-PL) and silk-poly-L-glutamic acid (SF-PG) with positive and negative charges, correspondingly, were alternatively deposited onto silica spheres with a polyethylenimine (PEI) prime layer to facilitate the LbL process. The LbL assembly of PEI-(SF-PG/SF-PL)<sub>n</sub> employed the same procedure as described above for the fabrication of (SF-PL/GO)<sub>n</sub> microcapsule.

**Zeta-Potential Measurements:** Zeta-potential after each deposited layer was measured on a Zetasizer Nano-ZS (Malvern) by averaging three independent measurements.

**Atomic Force Microscopy (AFM), Scanning Electron Microscopy (SEM) and Transmission Electron Microscopy (TEM):** Shell morphology was characterized on AFM in dry state. Tapping mode was utilized for collecting the topographical and phase images by using a silicon V-shape cantilevers with a spring constant of 46 N/m on Dimension-3000 (Digital Instruments). The capsule single wall thickness was analyzed by NanoScope software, calculated as half

of the height of the collapsed flat regions.<sup>[44,45]</sup> SEM images were collected from Hitachi S-3400-|| scanning electron microscope at a voltage of 10 kV. TEM imaging was performed on a JEOL 100CX operated at 100 kV by using a carbon-formvar TEM grid (Electron Microscopy Sciences).

*Raman imaging and Confocal Laser Scanning Microscopy (CLSM):* Raman spectra were collected utilizing a Witec (Alpha 300R) Confocal Raman Microscope equipped with a 514 nm Ar-ion laser. The images were collected with a 100x objective (NA = 0.75) with spectral resolution of 4 cm<sup>-1</sup>.

Confocal images of capsules were visualized by staining the shell with fluorescent isothiocyanate solution (prepared in phosphate buffer at pH 5.5) collected from LSM 510 Vis confocal microscopy equipped with 63 × 1.4 oil immersion objective lens (Zeiss) at 488/515 nm. FITC-Dextran solutions with different molecule weight (1 mg/mL in phosphate buffer) were used for measuring the capsule permeability at different pHs. Briefly, a drop of capsule suspension was added to Lab-Tech chamber (Electron Microscopy Science), then the chamber was half filled with FITC-Dextran solution, and waited for at least 30 mins for the capsules to settle down.

To investigate the mechanical properties of capsules by osmotic pressure measurement, a volume of capsule suspension was added to Lab-Tek chambers and mixed with a small amount of FITC-Dextran solution (50 μL, MW 2000 kDa). The chamber was filled with a volume of 2000 kDa dextran solution with different concentrations, prepared with phosphate buffer at pH 5.5, resulting in the required concentration of dextran in the chambers. For the osmotic pressure measurements, samples were prepared 12 hrs prior to observation by confocal microscopy

## Acknowledgement

The authors acknowledge technical support from Sidney T. Malak and Kesong Hu and funding from the Air Force Office for Scientific Research with FA9550-11-1-0233, FA9550-14-1-0015 and FA9550-09-1-0162 (BIONIC Center) Grants, China Scholarship Council grant 2010832447, and the priority academic program development of Jiangsu Higher education institutions, PAPD.

- [1] K. S. Novoselov, A. K. Geim, S. V. Morozov, D. Jiang, Y. Zhang, S. V. Dubonos, I. V. Grigorieva, A. A. Firsov, *Science* **2004**, *206*, 666.
- [2] K. S. Novoselov, A. K. Geim, S. V. Morozov, D. Jiang, M. I. Katsnelson, I. V. Grigorieva, S. V. Dubonos, A. A. Firsov, *Nature* **2005**, *438*, 197.
- [3] C. N. R Rao, A. K. Sood, K. S. Subramanyam, A. Govindraj, *Angew. Chem. Int. Ed.* **2009**, *28*, 7752.
- [4] A. K. Giem, S. K. Novoselov, *Nat. Mater.* **2007**, *6*, 183.
- [5] J. S. Bunch, V. Zande, S. S. Verbridge, I. W. Frank, D. M. Tanebaum, J. M. Parpia, H. G. Craighead, P. L. McEuen, *Science* **2007**, *315*, 490.
- [6] S. Stankovich, D. A. Dikin, G. H. B. Dommett, K. M. Kohlhaas, E. J. Zimmney, E. A. Stach, R. D. Piner, S. T. Nguyen, R. S. Ruoff, *Nat. Nanotechnol.* **2009**, *4*, 217.
- [7] T. K. Hong, D. W. Lee, H. J. Choi, H. S. Shin, B.-S. Kim, *ACS Nano* **2010**, *4*, 3861.
- [8] C. A. Merchant, K. Healy, M. Wanunu, V. Ray, N. Peterman, J. Bartel, M. D. Fischbein, K. Venta, Z. T. Luo, A. T. C. Johnson, M. Drndić, *Nano Lett.* **2010**, *10*, 2915.
- [9] B. G. Choi, M. Yang, W. H. Hong, J. W. Choi, Y. S. Huh, *ACS Nano* **2012**, *5*, 4020.
- [10] Q. Shao, J. Tang, Y. Lin, F. Zhang, J. Yuan, H. Zhang, N. Shinya, L. Qin, *J. Mater. Chem. A.* **2013**, *1*, 15423.
- [11] W. S. Hummers, R. E. Offeman, *J. Am. Chem. Soc.* **1958**, *80*, 1339.
- [12] K. Hu, D. D. Kulkarni, I. Choi, V. V. Tsukruk, *Prog. Polym. Sci.* **2014**, <http://dx.doi.org/10.1016/j.progpolymsci.2014.03.001>.
- [13] D. R. Dreyer, S. Park, C. W. Bielawski, R. S. Ruoff, *Chem. Soc. Rev.* **2010**, *39*, 228.
- [14] C. Li, J. Adamcik, R. Mezzenga, *Nat. Nano.* **2012**, *7*, 421.
- [15] D. Li, M. B. Müller, S. Gilje, R. B. Kaner, G. G. Wallace, *Nat. Nano.* **2008**, *3*, 101.
- [16] M. J. Allen, V. C. Tung, R. B. Kaner, *Chem. Rev.* **2010**, *110*, 132.
- [17] G. Eda, M. Chhowalla, *Adv. Mater.* **2010**, *22*, 2392.
- [18] X. Huang, X. Qi, F. Boey, H. Zhang, *Chem. Soc. Rev.* **2012**, *41*, 666.
- [19] L. Feng, L. Wu, X. Qu, *Adv. Mater.* **2013**, *25*, 168.
- [20] Y. Song, K. Qu, C. Zhao, J. Ren, X. Qu, *Adv. Mater.* **2010**, *22*, 2206.
- [21] C. Gómez-Navarro, M. Burghard, K. Kern, *Nano Lett.* **2008**, *8*, 2045.
- [22] J. W. Suk, R. D. Piner, J. An, R. S. Ruoff, *ACS Nano* **2010**, *4*, 6557.
- [23] D. D. Kulkarni, I. Choi, S. S. Singamaneni, V. V. Tsukruk, *ACS Nano* **2010**, *8*, 4667.
- [24] K. Hu, M. K. Gupta, D. D. Kulkarni, V. V. Tsukruk, *Adv. Mater.* **2013**, *25*, 2301.
- [25] J. Cao, Y. Wang, P. Xiao, Y. Chen, Y. Zhou, J. Ouyang, D. Jia, *Carbon* **2013**, *56*, 383.
- [26] K. Sohn, Y. J. Na, H. Chang, K.-M. Roh, H. D. Jang, J. Huang, *Chem. Commun.* **2012**, *48*, 5968.
- [27] J. Hong, K. Char, B.-S. Kim, *J. Phys. Chem. Lett.* **2010**, *1*, 3442.
- [28] S. A. Ju, K. Kim, J.-H. Kim, S.-S. Lee, *ACS Appl. Mater. Interfaces* **2011**, *3*, 2904.
- [29] R. Kurapati, A. M. Raichur, *Chem. Commun.* **2012**, *48*, 6013.
- [30] A. G. Skirtach, P. Karageorgiev, M. F. Bedard, G. B. Sukhorukov, H. Mohwald, *J. Am. Chem. Soc.* **2008**, *130*, 11572.
- [31] A. L. Becker, A. P. R. Johnston, F. Caruso, *Small* **2010**, *6*, 1836.
- [32] Z. H. Lu, M. D. Prouty, Z. H. Guo, V. O. Golub, C. Kumar, Y. M. Lvov, *Langmuir* **2005**, *21*, 2042.
- [33] K. Katagiri, K. Koumoto, S. Iseya, M. Sakai, A. Matsuda, F. Caruso, *Chem. Mater.* **2009**, *21*, 195.
- [34] M. N. Antipina, G. B. Sukhorukov, *Adv. Drug Delivery Rev.* **2011**, *63*, 716.
- [35] K. Hu, L. S. Tolentino, D. D. Kulkarni, C. Ye, S. Kumar, V. V. Tsukruk, *Angew. Chem. Int. Ed.* **2013**, *52*, 13784.
- [36] M. A. Serban, D. L. Kaplan, *Biomacromolecules* **2010**, *11*, 3406.
- [37] A. R. Murphy, P. St John, D. L. Kaplan, *Biomaterials* **2008**, *29*, 2829.
- [38] V. Kozlovskaya, E. Kharlampieva, M. L. Mansfield, V. Sukhishvili, *Chem. Mater.* **2006**, *18*, 328.
- [39] A. L. Becker, A. N. Zelikin, A. P. R. Johnston, F. Caruso, *Langmuir* **2009**, *25*, 14079.
- [40] V. Kozlovskaya, E. Kharlampieva, K. Jones, Z. Lin, V. V. Tsukruk, *Langmuir* **2010**, *26*, 7138.
- [41] Y. J. Wang, F. Caruso, *Chem. Commun.* **2004**, *13*, 1528.
- [42] K. Shimizu, J. Cha, G. D. Stucky, D. E. Morse, *Proc. Natl. Acad. Sci. USA* **1998**, *95*, 6234.
- [43] C. Ye, O. Shchepelina, R. Calabrese, I. Drachuk, D. L. Kaplan, V. V. Tsukruk, *Biomacromolecules* **2011**, *12*, 4319.
- [44] N. Elsner, F. Dubreui, A. Fery, *Phys. Rev. E* **2004**, *69*, 031802/1.
- [45] M. E. Mcconney, S. S. Singamaneni, V. V. Tsukruk, *Polymer Rev.* **2010**, *50*, 235.
- [46] S. Park, R. S. Ruoff, *Nat. Nanotechnol.* **2009**, *4*, 217.
- [47] A. K. Mkhoyan, A. W. Contryman, J. Silcox, D. A. Stewart, G. Eda, C. Mattevi, S. Miller, M. Chhowala, *Nano Lett.* **2009**, *9*, 1058.
- [48] W. M. Haynes, *Handbook of Chemistry and Physics*, 94th Ed., CRC Press, Boca Raton **2013**.

- [49] A. Yu, I. R. Gentle, G. Q. Lu, *J. Colloid Interface Sci.* **2009**, *333*, 341.
- [50] O. I. Vinogradova, *J. Phys: Condens. Matter* **2004**, *16*, R1105.
- [51] J. Heuvingh, M. Zappa, A. Ferry, *Langmuir* **2005**, *21*, 3165.
- [52] I. K. Moon, J. Lee, R. S. Ruoff, H. Lee, *Nat. Commun.* **2010**, *1*, 73.
- [53] D. D. Kulkarni, S. Kim, M. Chyasnachyus, K. Hu, A. G. Fedorov, V. V. Tsukruk, *J. Am. Chem. Soc.* **2014**, *136*, 6546.
- [54] O. Shchepelina, I. Drachuk, M. K. Gupta, J. Lin, V. V. Tsukruk, *Adv. Mater.* **2011**, *23*, 4655.
- [55] C. Jiang, X. Wang, R. Gunawidjaja, Y. H. Lin, M. K. Gupta, D. L. Kaplan, R. R. Naik, V. V. Tsukruk, *Adv. Funct. Mater.* **2007**, *17*, 2229.
- [56] E. Kharlampieva, V. Kozlovskaya, B. Wallet, V. V. Shevchenko, R. R. Naik, R. Vaia, D. L. Kaplan, V. V. Tsukruk, *ACS Nano* **2010**, *4*, 7053.
- [57] C. Porcel, Ph. Lavallo, V. Ball, G. Decher, B. Senger, J.-C. Voegel, P. Schaaf, *Langmuir* **2006**, *22*, 4376.
- [58] Ph. Lavallo, C. Picart, J. Mutterer, C. Gergely, H. Reiss, J. C. Voegel, B. Senger, P. Schaaf, *J. Phys. Chem. B* **2004**, *108*, 635.
- [59] R. Robitaille, F. A. Leblond, Y. Bourgeois, N. Henley, M. Loignon, J.-P. Hallé, *J. Biomed. Mater. Res.* **2000**, *50*, 420.
- [60] K. D. Hermanson, M. B. Harasim, T. Scheibel, A. R. Bausch, *Phys. Chem. Chem. Phys.* **2007**, *9*, 6442.
- [61] C. Ye, I. Drachuk, C. Rossella, H. Dai, D. L. Kaplan, V. V. Tsukruk, *Langmuir* **2012**, *28*, 12235.
- [62] J. K. Armstrong, R. B. Wenby, H. J. Meiselman, T. C. Fisher, *Biophys. J.* **2004**, *87*, 4259.
- [63] J. M. G. Cowie, V. Arrighi, *Polymers: Chemistry and Physics of Modern Materials*, 3rd Ed., CRC Press, Boca Raton, USA **2008**.
- [64] C. A. Daniels, *Polymers: Structure and Properties*. Technomic Publishing Company, Lancaster, Pennsylvania **1989**.
- [65] N. Laugel, C. Betscha, M. Winterhalter, J. C. Voegel, P. Schaaf, V. Ball, *J. Phys. Chem. B* **2006**, *110*, 19443.
- [66] I. Choi, R. Suntivich, F. A. Plamper, V. Snatschke, A. H. E. Müller, V. V. Tsukruk, *J. Am. Chem. Soc.* **2011**, *133*, 9592.
- [67] V. A. Parsegian, R. P. Rand, N. L. Fuller, D. C. Rau, *Methods Enzymol.* **1986**, *127*, 400.
- [68] F. Vérétoit, M. Delaye, A. Tardieu, *J. Mol. Biol.* **1989**, *205*, 713.
- [69] M. P. Tombs, A. R. Peacocke, *The Osmotic Pressure of Biological Macromolecules*, Oxford University Press, London **1974**.
- [70] C. Gao, E. Donath, S. Moya, V. Dudnik, H. Mohwald, *Eur. Phys. J. E.* **2001**, *5*, 21.
- [71] C. Gao, S. Leporatti, S. Moya, E. Donath, H. Mohwald, *Langmuir* **2001**, *17*, 3491.
- [72] C. Bonnet-Gonnet, L. Belloni, B. Cabane, *Langmuir* **1994**, *10*, 4012.
- [73] B. Sierra-Martin, J. A. Frederick, Y. Laporte, G. Markou, J. J. Lietor-Santos, A. F. Fernandez-Nieves, *Colloid Polym. Sci.* **2011**, *289*, 721.
- [74] T. Boudou, T. Crouzier, R. Auzély-Velty, K. Glinel, C. Picart, *Langmuir* **2009**, *25*, 13809.
- [75] L. D. Landau, E. M. Lifshitz, *Theory of Elasticity*, 3rd Ed., Elsevier Butterworth-Heinemann, Oxford **1997**.
- [76] A. V. Pogorelov, *Bending of Surface and Stability of Shells*, American Mathematical Society, Rhode Island **1988**.
- [77] T. Boudou, T. Crouzier, R. Auzély-Velty, K. Glinel, C. Picart, *Langmuir* **2009**, *25*, 13809.
- [78] I. Drachuk, O. Shchepelina, M. O. Lisunova, S. Harbaugh, N. Kelley-Loughnane, M. Stone, V. V. Tsukruk, *ACS Nano* **2012**, *5*, 4266.
- [79] M. O. Lisunova, I. Drachuk, O. Shchepelina, K. D. Anderson, V. V. Tsukruk, *Langmuir* **2011**, *27*, 11157.
- [80] O. Shchepelina, M. O. Lisunova, I. Drachuk, V. V. Tsukruk, *Chem. Mater.* **2012**, *24*, 1245.
- [81] C. Jiang, V. V. Tsukruk, *Adv. Mater.* **2006**, *18*, 829.
- [82] O. I. Vinogradova, D. Andrienko, V. V. Lulevich, S. Nordschild, G. B. Sukhorukov, *Macromolecules* **2004**, *37*, 1113.
- [83] A. Fery, V. V. Tsukruk, in *Multilayer Thin Films*, (Eds. G. Decher, J. Schlenoff), Wiley-VCH, Weinheim **2012**, 363.
- [84] L. H. Sperling, *Polymeric Multicomponent Materials*, Wiley-VCH, New York **1997**.
- [85] M. F. Bédard, A. Munoz-Javier, R. Mueller, P. D. Pino, A. Fery, W. J. Parak, A. G. Skirtach, G. B. Sukhorukov, *Soft Matter* **2009**, *5*, 148.
- [86] G. B. Sukhorukov, H. Möhwald, *Trends Biotechnol.* **2007**, *25*, 93.

Received: April 22, 2014  
Revised: June 26, 2014  
Published online: August 8, 2014